Effect of fluctuations in the down ramp plasma source profile on the emittance and current profile of the self-injected beam in a plasma wakefield accelerator

C. Zhang, C.K. Huang, K.A. Marsh, X.L. Xu, F. Li, M. Hogan, V. Yakimenko, S. Corde, W.B. Mori, C. Joshi

Effect of fluctuations in the down ramp plasma source profile on the emittance and current profile of the self-injected beam in a plasma wakefield accelerator

C. Zhang,[1] C.-K. Huang,[1] K. A. Marsh,[1] X. L. Xu,[2] F. Li,[1] M. Hogan,[2] V. Yakimenko,[2] S. Corde,[3] W. B. Mori,[1] and C. Joshi[1]

[1]*University of California Los Angeles, Los Angeles, California 90095, USA*
[2]*SLAC National Accelerator Laboratory, Menlo Park, California 94025, USA*
[3]*LOA, ENSTA Paris, CNRS, École Polytechnique, Institut Polytechnique de Paris, 91762 Palaiseau, France*

(Received 3 July 2019; published 4 November 2019)

With its extreme beam parameters, the FACET II facility enables the test of the down ramp injection scheme in the laboratory for the beam-driven plasma wakefield accelerator approach. In addition to the ideal cases studied in previous theoretical work, we investigate the effect of fluctuations in the down ramp plasma source profile on the emittance and current profile of the self-injected beam using 2D and 3D particle-in-cell simulations. We show that down ramps with a length of $\sim 10\ c/\omega_p$ can be reproducibly created by generating a shock in a supersonic flow. Simulations show that the emittance of the injected beam using such down ramps is $\sim 0.1\ \mu$m. A gentler ramp can further reduce the slice emittance of the beam to $\sim 0.03\ \mu$m. The emittance of the injected beam depends on the ramp length but is insensitive to the shape of the ramp. However, the current profile of the injected beam can be manipulated by changing the ramp shape. A simulation shows that, when a noncylindrical driver is used, the emittance of the injected beam differs in the two orthogonal transverse planes and is a few times larger than that of the cylindrical driver case. A full-scale simulation where we use a realistic density profile that includes the up ramp, the injecting down ramp, and the exiting down ramp is presented to show that the beam emittance is preserved during the acceleration and extraction of the beam.

DOI: 10.1103/PhysRevAccelBeams.22.111301

I. INTRODUCTION

The rapid development of plasma-based accelerators is opening new possibilities in both fundamental and applied research by providing tools of scientific discovery. For instance, the demonstration of high-quality, high-efficiency acceleration of both electrons [1–3] and positrons [4] raises hopes for a plasma-based next-generation collider [5], while compact coherent and incoherent x- and γ-ray sources based on ultrabright beams enabled by plasma accelerators [6–10] may find broad applications in material, chemical, and biological sciences [11–13]. Both tools of scientific discovery require the generation of ultralow-emittance, high-brightness beams [5,6,14,15] which have not been demonstrated to date in plasma acceleration experiments, and, thus, this topic is being actively studied.

Different methods for generating ultralow-emittance, high-brightness beams from plasma-based accelerators have been proposed and investigated using particle-in-cell (PIC) simulations. One of these methods uses one [16–18] or two laser pulses [19] to ionize a high-Z gas inside the accelerating cavity that resembles a "bubble" produced by either a laser or a particle beam driver to trigger ionization injection [20–22]. Simulations show that, using this scheme, the emittance of the injected beam can be as low as ~ 10 nm, and the brightness can reach $\sim 10^{19}$ A/m^2/rad^2 [19]. However, this scheme puts critical requirements on the spatiotemporal synchronization of the ionization laser(s) and the drive beam, which makes it very challenging to implement in the laboratory. Recently, it was proposed that self-injection triggered by a density down ramp has the potential of generating electron beams with a slice emittance also as low as ~ 10 nm and a brightness up to 10^{21} A/m^2/rad^2 [23]. This method is more appealing due to its relative simplicity. Laser-driven down ramp injection has been used [24–28] to generate low-energy-spread electron beams with an emittance on the order of $\sim 1\ \mu$m [26]; however, the down ramp injection scheme has not yet produced ultralow ($\ll 1\ \mu$m), high-brightness

($>10^{18}$ A/m^2/rad^2) beams. Previous work [23] showed that the emittance of the injected bunch from down ramp trapping critically depends on the adiabatic deceleration process in the radial direction at the very back of the bubble, and such a deceleration process should be cylindrically symmetric to minimize the emittance of the injected bunch. In other words, the driver (either a laser or a particle beam) should be such that it is able to excite a cylindrically symmetric wake. A possible reason why electron bunches with ultralow emittance were not observed in previous experiments using laser drivers might be that this requirement on the injection process was not met, since the trajectories of the sheath electrons strongly depend on the local intensity of the laser pulse [29]. On the other hand, although being actively pursued at major facilities [30,31], the concept of generating ultralow-emittance beams using down ramp injection in a plasma wakefield accelerator has not been demonstrated in experiments. To test this injection scheme using the extreme beams available at FACET II [32], there are still open questions in implementing this method. The most critical question is do the fluctuations in the drive electron beam or the plasma source parameters affect the reproducibility of the results? In this paper, we present simulation results to address the latter part of the question, namely, to show the effects of the plasma source itself on the sensitivity and reproducibility of the down ramp injection. To this end, we have characterized the reproducibility of the density down ramps of interest and then used particle-in-cell code simulations to quantify fluctuations of the emittance of the injected beam and its growth during the acceleration process and eventual extraction using a second longer down ramp that acts as a matching section.

In this article, we first show that, by introducing a shock in a supersonic flow, a density down ramp can be reproducibly created. The upper shelf and the lower shelf densities of the ramp can be continuously tuned in the range of 10^{18}–10^{19} cm^{-3}. The ramp length is $\sim 10\ c/\omega_p$ under the conditions of interest. Here $\omega_p = \sqrt{e^2 n_p/\varepsilon_0 m_e}$ is the plasma frequency, and n_p is the lower shelf density of the ramp. We show using 3D PIC simulations that, by utilizing a drive beam with the FACET II nominal parameters [32], electron beams with a slice emittance as low as ~30 nm can be injected. The peak current of the injected beam is ~10 kA, corresponding to a peak brightness of 10^{19} A/m^2/rad^2. Simulations show that a sharper (gentler) ramp leads to the injection of beams with a larger (smaller) slice emittance. We also show that the slice emittance of the injected beam is insensitive to the ramp shape but depends on the ramp length for given densities. On the contrary, the current profile of the injected beam depends on the ramp shape but is insensitive to the ramp length. The emittance of the injected beam becomes larger when the drive beam is noncylindrical—the emittance increases by a factor of ~10 for the driver with a transverse beam size ratio of 1.5. Finally, we show through a 2D simulation that the emittance of the injected beam is preserved in the acceleration and the matching section, which makes it possible to capture, transport, and characterize the beam downstream using conventional beam diagnostics.

II. REPRODUCIBLE DOWN RAMP PLASMA SOURCE

A relatively simple method to create a sharp density down ramp is to generate a shock by inserting a blade to perturb a supersonic flow [24,25] typically emanating from a gas jet. We have experimentally studied the creation of such down ramps. The schematic of the experimental setup is shown in Fig. 1(a). The conical nozzle used in this experiment has a 0.5-mm-diameter entrance which is connected to a pulsed solenoid valve (not shown) and a 4-mm-diameter exit. The length of the nozzle is 5 mm, and, therefore, the half opening angle of the nozzle is 19.3°. A thin blade (surgical scalpel blade No. 11) is inserted into the supersonic flow to create a shock wave that creates a density jump—the density first increases compared to the density without the blade and then sharply drops,

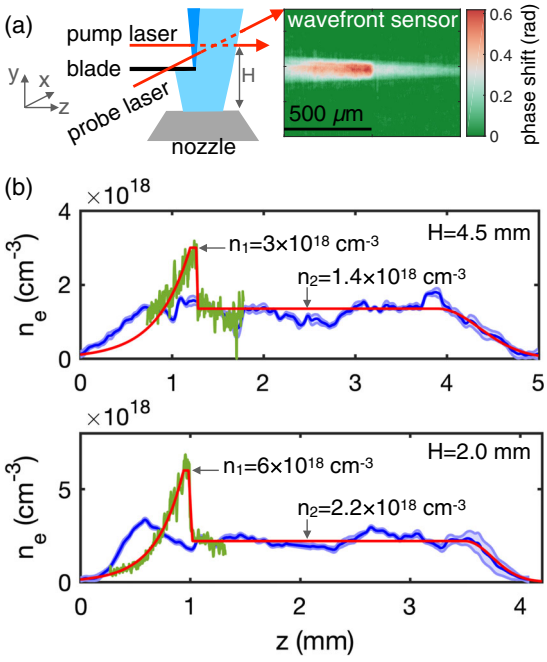

FIG. 1. Schematic of the experimental setup (a) and the measured density profiles (b). The plasma density was measured using a wave front sensor, and a representative phase map is shown in (a). The blue lines in (b) show the measured density profiles without a blade (averaged over 20 shots, synthesized using 4–5 frames in the z direction due to the ~1-mm-wide view of the camera) at different heights above the nozzle exit. The shaded region represents the standard deviation. The green lines are the measured density profiles with a blade inserted (single shot). The red lines are simplified density profiles used in simulations.

producing the density down ramp. The distance between the blade and the nozzle exit was fixed to ∼0.7 mm in the experiment. The height of the pump laser was changed from 2 to 4.5 mm by moving the nozzle vertically. A small portion (∼1%) of the pump laser was split off and was used as a probe beam which traversed the plasma at the right angle with a <3 ps delay. A wave front sensor (Phasics SID4-HR-GE) was used to measure the phase shift induced by the plasma, and a representative phase map is shown in Fig. 1(a). The image clearly shows a sudden change in the middle of the phase map, which indicates the position of the shock front. On the left-hand side, the flow is retarded by the blade and, thus, has a smaller Mach number and consequently a higher density.

The measured plasma density profiles are shown in Fig. 1(b). The blue lines show the density profiles measured at two different heights above the nozzle exit without the blade. In each plot, the solid blue line is an average over 20 shots, and the shaded region represents the standard deviation. It can be seen that the unperturbed density profile consists of a ∼3 mm flat region and ∼0.5 mm ($H = 2$ mm case) or ∼1 mm ($H = 4.5$ mm case) ramps on both sides. The green lines are measured density profiles with the blade inserted. In these measurements, the blade was ∼0.7 mm above the nozzle and covered ∼1 mm (measured from the edge) of the nozzle. Under these conditions, the shock front was perpendicular to the propagation direction of the pump laser, as can be seen in the phase map in Fig. 1(a). This allowed us to retrieve the density from the measured phase shift using Abel inversion. For other blade coverages, the shock front was oblique with respect to the flow direction. The green lines extend over 1.1 mm, which was limited by the field of view of the Phasics camera. We have confirmed in the experiment that the plasma remained unchanged in the lower-density side of the shock [within the variation shown by the blue shaded area in Fig. 1(b)], as evidenced by the very good agreement between the measured density with (green lines) and without (blue lines) the blade. The red lines in Fig. 1(b) are simplified density profiles used in simulations as will be discussed later.

To investigate tunability of the down ramp created using this method, we changed the backing pressure of the gas jet. In Fig. 2, the upper shelf density (a), the lower shelf density (b), and the ramp length in real units (c) and normalized units (d) are plotted as functions of the backing pressure. These data were measured with a plasma height (distance between the pump laser and the nozzle exit) of ∼2 mm. The results show that both the upper shelf and the lower shelf densities of the down ramp can be tuned almost linearly by changing the backing pressure. Within the backing pressure range we used, the lower shelf density changes from 1.5 to 4×10^{18} cm^{-3}, and the density drops by a factor of 2–3 across the shock front. The lower limit of the density was predominantly determined by the sensitivity of the wave front sensor, and the upper limit was due to the working

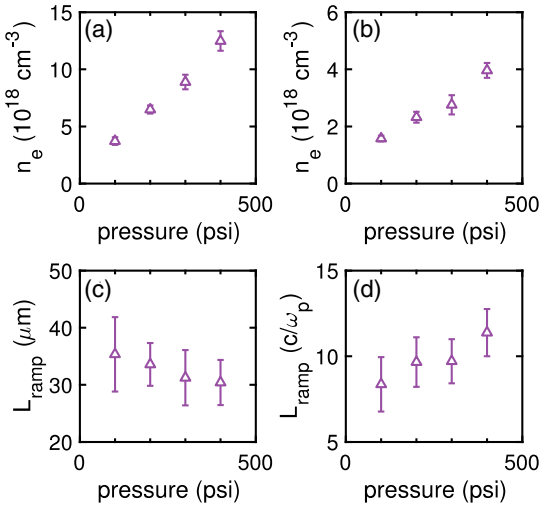

FIG. 2. Characteristics of the down ramp as a function of the backing pressure. (a) Upper shelf density of the down ramp. (b) Lower shelf density of the down ramp. (c) Ramp length in real units. (d) Ramp length in normalized units. Each data point is an average, and the error bar represents the standard deviation of 20 shots.

range of our gas regulator. In principle, however, it is possible to extend the density range further down to a few times of 10^{17} cm^{-3} and up to 10^{19} cm^{-3}. The average length of the ramp remains almost constant (∼30 μm or ∼10 c/ω_p) under these conditions.

In the experiment, we also changed the height of the plasma by moving the nozzle and the blade vertically. Figure 3 shows the characteristics of the down ramp as a

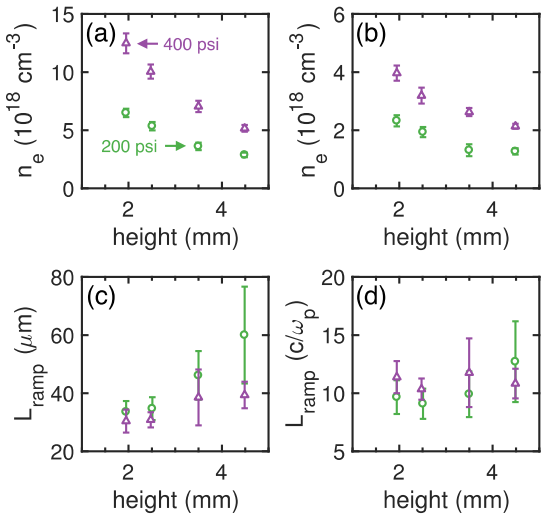

FIG. 3. Characteristics of the down ramp as a function of the plasma height. (a) Upper shelf density of the down ramp. (b) Lower shelf density of the down ramp. (c) Ramp length in real units. (d) Ramp length in normalized units. Each dot is an average, and the error bar represents the standard deviation of 20 shots. The purple triangles (green circles) are measured under a backing pressure of 400 (200) psi.

function of the plasma height. When changing the plasma height, the distance between the blade and the nozzle exit was kept at ∼0.7 mm. The data show that, for a given backing pressure, the density drops as the height increases as expected. Figures 3(c) and 3(d) show the ramp length in real and normalized units, respectively. The ramp length in real units increases slightly as the height increases but remains ∼10 c/ω_p, because the density drops for a larger height. Therefore, we conclude that the down ramp across a shock front created by inserting a blade into a supersonic flow has a length of ∼10 c/ω_p within the density range of 10^{18}–10^{19} cm^{-3} for the nozzle we used. The measured ramp length fluctuates on a ∼20% level from shot to shot. One possible reason might be the fluctuation of the gas flow from the nozzle with respect to the blade. In the experiment, we observed an ∼100 μm fluctuation of the shock front position in the propagation direction of the ionizing laser which may be attributed to the nozzle and the blade being mounted separately. We note that down ramps can also be created using optical methods [33,34] with comparable parameters as those created using hydrodynamics-based methods.

III. SENSITIVITY OF RAMP VARIATIONS ON EMITTANCE AND CURRENT PROFILE

In the following part of the paper, we will show the sensitivity of ramp variations on emittance and current profile of the injected beam. Theoretical work [23] showed that the down ramp injection scheme has the potential of generating ultralow-emittance (∼10 nm) beams. The wake elongates, and, therefore, its effective phase velocity ($v_{\rm ph}$) drops as the drive beam traverses through the down ramp. As the sheath electrons move backwards in the frame of the wake, they gain energy and will be trapped by the wake if their longitudinal velocity becomes larger than $v_{\rm ph}$. At the same time, the transverse momentum of most of the electrons reaching the back of the bubble increases dramatically due to the large focusing force from the ion column. However, a careful analysis shows that the transverse momentum of the injected electrons is actually greatly reduced by the high charge and current densities in a small region at the very back of the bubble, which makes it possible to generate ultralow-emittance beams [23]. Under the right conditions, the injected electrons in fact have almost zero transverse residual momentum, which leads to a very low emittance. This deceleration process should better be adiabatic to minimize the residual transverse momentum of the injected electrons. In other words, a gentle ramp ($L_{\rm ramp} \gg c/\omega_p$) is preferable for injecting ultralow-emittance beams.

As mentioned in the previous section (Figs. 3 and 4), the ramp length under the conditions of interest varies in the range of ∼5–15 c/ω_p. Therefore, we have performed 3D PIC simulations using the OSIRIS [35] code to investigate

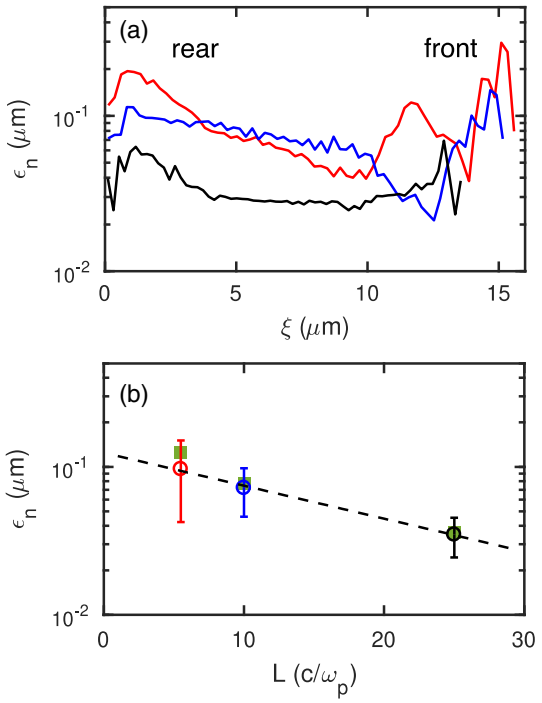

FIG. 4. Emittance of the injected beam for three different ramp lengths. The upper and lower shelf densities are 6 and 2.2×10^{18} cm^{-3}, respectively, and the ramp length changes from 5 to 25 c/ω_p. The slice emittance of the injected beam is shown in (a) for $L = 5c/\omega_p$ (red), $L = 10\ c/\omega_p$ (blue), and $L = 25\ c/\omega_p$ (black). The front of the injected beam is marked in (a). The average and standard deviation of the slice emittance of the injected beam are shown in (b) by circles and error bars, respectively. The green squares show the projected emittance of the injected beam. The dashed line is the best linear fit to the slice emittance data. The emittance is evaluated after the beam being accelerated for ∼100 c/ω_p so that the beam has gained a moderate energy ($\bar{\gamma} \approx 74$).

the sensitivity of the ramp length on the emittance of the injected beam. The results are shown in Fig. 4. In these simulations, the upper shelf density is 6×10^{18} cm^{-3}, and the lower shelf density is 2.2×10^{18} cm^{-3} (the red line in the bottom plot in Fig. 1(b)]. The driver has a bi-Gaussian shape with a length of $\sigma_z = 3$ μm and a transverse size of $\sigma_r = 5$ μm. The normalized peak current of the driver is $\Lambda \equiv \frac{n_b}{n_p}(k_p\sigma_r)^2 = 4$. Here n_b is the peak density of the driver, n_p is the lower shelf density of the down ramp, and $k_p\sigma_r$ is the normalized radius of the driver. The simulation box has a length of 13 c/ω_p in the z direction along which the box moves at the speed of light. In the other two orthogonal directions, the box is 16 c/ω_p wide. The cell size is $1/40$ c/ω_p in all three directions, and eight electrons are initialized in each cell. Immobile ions serve as a charge-neutralizing background. Figure 4(a) shows the normalized slice emittance of the injected beam in three cases where the ramp lengths are 5 (red line), 10 (blue line), and 25 c/ω_p (black line), respectively. In all three cases, the

beam is divided into 64 slices. Here the normalized emittance $\epsilon_n = \frac{1}{m_e c}\sqrt{x^2 p_x^2 - (x p_x)^2}$ is shown. Note that, instead of the usual unit of "mm mrad," the emittance is often characterized in the units of "μm." The data show that, even for the most abrupt down ramp ($L = 5\ c/\omega_p$), the slice emittance of the beam is about 0.1 μm. We note that simulations of laser-driven down ramp injection show that the generation of beams with an emittance as low as ~0.2 μm is achievable [36,37].

For gentler ramps, the slice emittance of the beam is further reduced to ~35 nm. The reason for this smaller emittance is attributed to the fact that in this gentler ramp case both the residual transverse momentum and the size of the injected beam are more likely to be adiabatically reduced to close to zero. The residual transverse momenta of the injected beams in the three cases with an increasing down ramp length (5, 10, and 25 c/ω_p) are 0.42, 0.34, and $0.24 m_e c$, respectively. These transverse momenta correspond to angular divergences of 5.7, 4.6, and 3.2 mrad, respectively. The transverse sizes of the injected beams are 0.30, 0.23, and 0.15 μm, respectively, which also decrease as the down ramp length increases. All these quantities are root-mean-square (rms) values and are evaluated after the beam has been accelerated for ~100 c/ω_p. Figure 4(a) also shows that for a given density down ramp the slice emittance of the injected bunch does not vary significantly through the whole bunch. The results suggest that the emittance of the bunch depends critically on the slope of the density down ramp. The average of the slice emittance is shown in Fig. 4(b) by the circles. The error bar shows the standard deviation. The green squares show the projected emittance of the beam. The dashed line shows the best linear fit to the slice emittance data. Interestingly, the data show that the emittance decreases almost exponentially as the down ramp length increases. We note that other numerical studies have shown contradictory results; i.e., the emittance of the injected beam either decreases [36] or increases [37] for a longer down ramp. This discrepancy as well as the exponential decrease of the emittance we observed are worth being checked in an experiment.

A fascinating feature of down ramp injection is that there is an almost linear correlation between the initial location of an electron before injection (z_i) and its final location in the injected bunch (ξ_f): $\frac{d\xi_f}{dz_i} \approx \frac{d\lambda_{\rm wake}}{dz_i} \approx 2\frac{dr_m}{dz_i}$, where $r_m \approx \lambda_{\rm wake}/2$ is the maximum bubble radius [23]. This linear correlation helps to avoid the longitudinal phase mixing that presents in ionization injection [17] and, therefore, enables the generation of ultralow slice emittance beams. On the other hand, the injected beam will have a linear energy chirp, because the electrons in the front of the injected beam are trapped earlier and, thus, have gained more energy by the end of the injection.

Such a correlation also makes it possible to control the current profile of the injected beam by changing the shape of the down ramp. Theory shows that the current of the injected beam can be approximated as $I(\xi)d\xi \approx ec2\pi r_i \Delta r_i n_p(z) dz_i$ [23]. Here $2\pi r_i \Delta r_i n_p dz_i$ is the number of injected electrons at z_i, and $d\xi$ is the length occupied by these electrons in the injected beam. All the injected electrons come from a small region with $r_i \approx \kappa r_m$, where $r_m \approx 2\sqrt{\Lambda}\frac{c}{\omega_p}$ is the radius of the bubble driven by an intense beam driver and $\kappa \approx \frac{1}{2}$ is an empirical constant. It can be seen that the current profile depends on the ramp shape $n_p(z)$. Figure 5 shows the current profiles of the injected beams where the ramps have the same parameters as those in Fig. 4. In these cases, the upper and the lower shelf densities are the same, and the ramps are linear. Therefore, the current profiles are similar. The peak current reaches 10 kA.

Examples with other ramp shapes are shown in Fig. 6. In Fig. 6(a), three different ramps used in the simulations are shown. In all three cases, the upper shelf density is $n_1 = 3.3 \times 10^{18}$ cm^{-3}, the lower shelf density is $n_2 = 2.2 \times 10^{18}$ cm^{-3}, and the length of the ramp is 30 c/ω_p. Here the density drop is smaller and the ramp length is longer than that used in previous simulations to lower the peak current of the injected bunch and, hence, to suppress the possible effects of beam loading on modifying the current profile of the bunch. We note that, in principle, the ramp length can be increased by rotating the nozzle-blade assembly so that the angle between the drive beam direction and the gas flow direction changes, and, therefore, the effective length of the down ramp changes. The blue line shows a $\sin^2$ ramp, $n_p(z) = n_1 - 0.5 n_2[\sin(\frac{\pi z}{2L})]^2$, where $L = 30\ c/\omega_p$ is the ramp length. The red and black lines represent the positive and negative parabolic ramps with $n_p(z) = n_2 + (n_1 - n_2)(z-L)^2/L^2$ and $n_p(z) = n_1 - (n_1 - n_2)z^2/L^2$, respectively. The same driver as in Fig. 4 was used. Figure 6(b) shows the slice emittance of the injected beam. The slice emittance is ~10 nm except for the front of the beam that corresponds to the positive

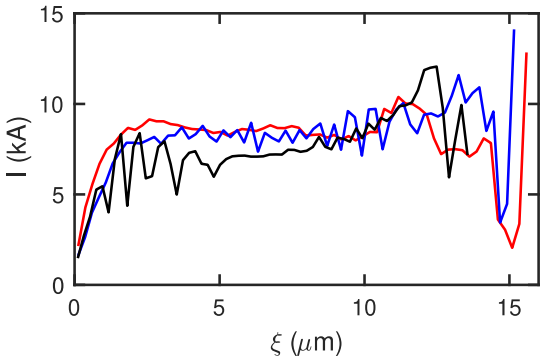

FIG. 5. Current profile of the injected beam. The ramp parameters are the same as those in Fig. 4. The red, blue, and black lines correspond to ramp length of 5, 10, and 25 c/ω_p, respectively.

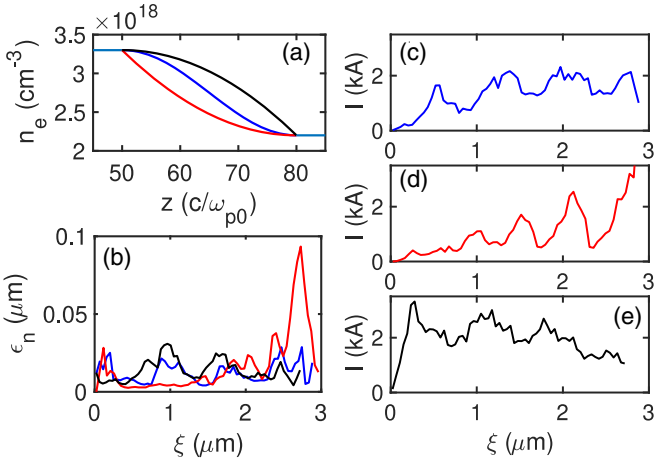

FIG. 6. Current profile and emittance of the injected beam for different ramp shapes. (a) Three different ramp shapes. (b) The normalized slice emittance of the injected beam for different ramp shapes. (c)–(e) Current profiles of the injected beams. In (b)–(e), the color of the lines corresponds to that in (a).

parabolic ramp [the red line in Fig. 6(a)], which is because the density drops so abruptly that the transverse momentum of the sheath electrons cannot be adiabatically reduced to near zero. Figures 6(c)–6(e) show the current profiles of the injected beam. The color code is the same as in Fig. 6(a). The results show that, for the $\sin^2$ ramp [blue line in Fig. 6(a)], the current profile is almost flat, which is consistent with the previous cases of the linear down ramp. The peak current is 2 kA, which is smaller than that in Fig. 5 due to the smaller density drop ($\Delta n = 1.1 \times 10^{18}\,\mathrm{cm}^{-3}$ compared against $\Delta n = 3.8 \times 10^{18}\,\mathrm{cm}^{-3}$). In both parabolic ramp cases, the current profile has an approximately triangular shape. The higher current part of the injected beam corresponds to the largest gradient part of the ramp. Figure 6(d) shows an interesting case where the beam current decreases almost linearly towards the back of the beam, which makes it suitable for achieving high beam loading efficiency [38–40], whereas the current profile shown in Fig. 6(e) is useful for high transformer ratio [41–44] wakefield acceleration.

IV. NONCYLINDRICAL DRIVER

In the above simulations, the driver is cylindrically symmetric. A noncylindrical driver will excite asymmetric wakes, which may not have the necessary structure to fully slow down the sheath electrons as they move towards the bubble axis when the injection occurs. Therefore, the emittance of the injected beam may increase. To quantify the effects of the noncylindrical driver, we have performed a 3D simulation where the ramp drops from a higher density of $n_1 = 3 \times 10^{18}\ \mathrm{cm}^{-3}$ to a lower density of $n_2 = 2.2 \times 10^{18}\ \mathrm{cm}^{-3}$ in 10 c/ω_p and the driver is now noncylindrical, i.e., $\sigma_x = 6.6\ \mu$m and $\sigma_y = 4.5\ \mu$m. Here x and y are the two orthogonal transverse planes. The peak current and the bunch length of the driver are unchanged. The simulation results are shown in Fig. 7 after the drive beam has propagated $\sim 100\ c/\omega_p$ in the lower shelf region.

Figures 7(a) and 7(b) show the plasma densities in the two orthogonal transverse planes. The bubble is broader in the x plane due to the larger spot size of the bunch in this direction. Figure 7(c) shows the slice emittance of the beam, where the red line is for ϵ_x and the blue line is for ϵ_y. Because of the asymmetric wake structure, the emittance of the beam differs in the two orthogonal transverse planes. Compared to the cylindrically symmetric driver case, the slice emittance has increased by a factor of ~ 10 to $\sim 1\ \mu$m. Another simulation with the same lower shelf density and down ramp length but a higher upper shelf density of $n_1 = 6 \times 10^{18}\ \mathrm{cm}^{-3}$ gives a similar emittance of $\sim 1\ \mu$m. These results suggest that controlling the cylindrical symmetry of the driver would be critical for generating ultralow-emittance beams which can be investigated in experiments.

V. FULL-SCALE SIMULATION

After the injection and acceleration, the low-emittance beam must be matched out from the plasma to the downstream conventional beam optics so that it can be characterized. It has been proposed that a properly tailored plasma section can be used as a matching section to gradually change the beta function of the beam so that its emittance is

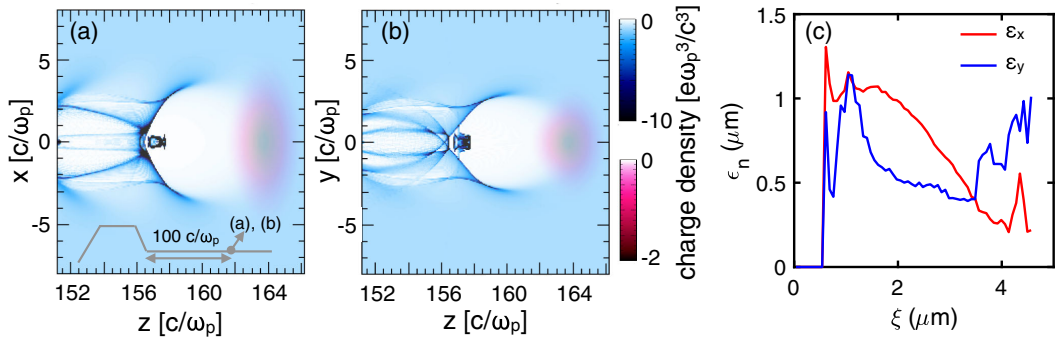

FIG. 7. Noncylindrical driver case. (a) and (b) are plasma densities in the transverse planes taken after the beam has been accelerated for $\sim 100\ c/\omega_p$, as indicated by the inset in (a). (c) The normalized slice emittance in the transverse planes.

preserved [45]. There is a natural down ramp at the edge of the gas jet which may be used as the matching section. To investigate this, we have performed a full-scale simulation using the simplified density profile [the red line in the bottom row in Fig. 1(b)] which includes the up ramp at the entrance, the injection down ramp, the acceleration section, and the matching down ramp at the exit. The simulation is a 2D slab due to the available computation resources. The peak density of the driver is reduced so that the current $\Lambda = 2$ to optimize the injection process. The results are shown in Fig. 8.

Figures 8(a)–8(c) show the plasma densities at three representative positions which correspond to the location of injection, the end of acceleration, and the matching section, respectively. The inset in Fig. 8(a) shows the plasma density profile used in the simulation [it is the measured but simplified profile as shown by the red line in the bottom row in Fig. 1(b)] and marks the locations where Figs. 8(a)–8(c) are taken. It can be seen from these density plots that, in this 2D simulation, different slices of the injected bunch undergo betatron oscillation with different frequencies because the bunch is not matched. At the exit of the plasma, the transverse size of the bunch has increased due to the decreasing of the focusing force. The corresponding longitudinal phase spaces of the bunch are shown in Figs. 8(d)–8(f). As expected, the bunch has a positive chirp (the front of the bunch has a higher energy), because the electrons in the front of the bunch are injected earlier and, thus, have been accelerated for a longer time. As the bunch is being accelerated, it rotates in the longitudinal phase space (LPS), since the back of the bunch feels a larger accelerating gradient as long as the wake is not overloaded. At the end of the flat region, the front part of the bunch (which contains most of the charge) has been flattened in the LPS, which leads to a narrow spike in the energy spectrum. In Figs. 8(d)–8(f), the blue lines show the current profile of the injected beam in arbitrary units. Results from 3D simulations using similar down ramp parameters (see Fig. 5) show that the peak current of the injected beam is ~10 kA. The peak energy of this spike is 0.2 GeV with a rms energy spread of ~3%. The bunch has a large negative chirp, which increases the projected energy spread; however, the slice energy spread remains as low as ~0.5% throughout the whole bunch, and it has been demonstrated that the negative chirp of the bunch can be removed by a plasma dechirper [46–48] so that the projected energy spread of the bunch can be reduced to be comparable to the slice energy spread. In another simulation where the length of the plasma is 2 cm, the peak energy of the beam exceeds 1 GeV.

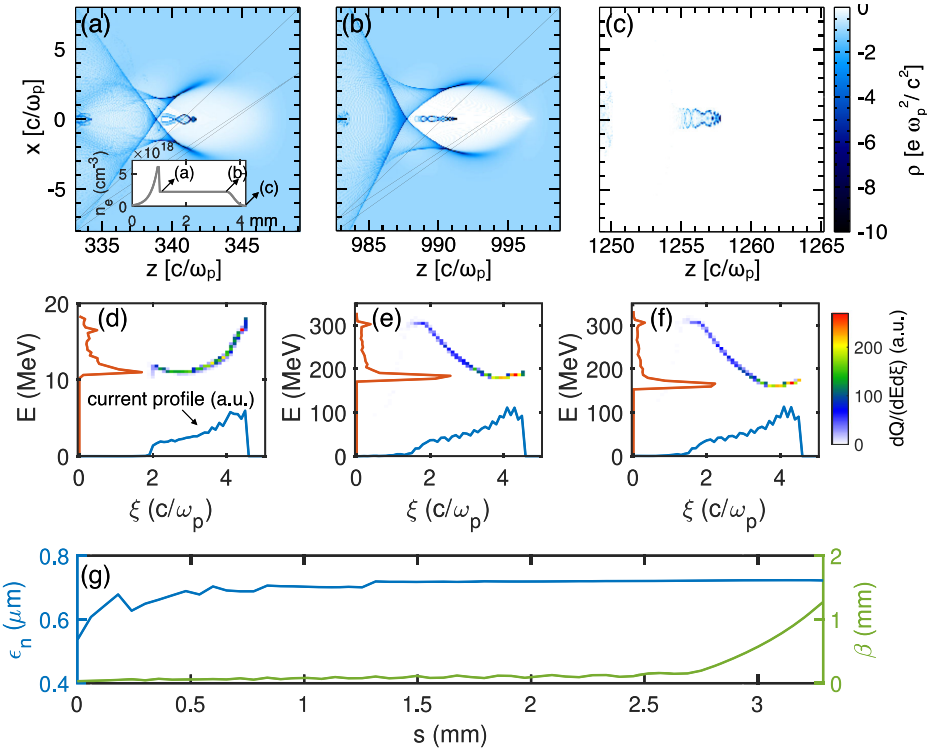

FIG. 8. Full-scale simulation including the injection, acceleration, and matching sections. (a)–(c) show the plasma density plots at positions marked in the inset in (a), which correspond to the position of injection, the end of acceleration, and the matching section. (d)–(f) show the longitudinal phase spaces of the injected bunch. The blue lines are the current profile in arbitrary units, and the red lines show the energy spectrum of the bunch. The blue (green) line in (g) shows the evolution of the average slice emittance (beta function) as a function of the acceleration distance.

The evolution of the average slice emittance and the beta function of the injected beam are shown in Fig. 8(g) by the blue and green lines, respectively. The results show that the emittance is preserved during the acceleration and the matching section. The emittance at the exit of the plasma is about 0.7 μm. The beam is tightly focused inside the bubble due to the strong focusing force and has a beta function of ~0.1 mm. The matching section almost adiabatically increases the beta function of the beam by more than an order of magnitude to ~1.2 mm so that the beam can be captured by the downstream focusing elements. We note that, because of the use of the natural down ramp at the edge of the nozzle, the matching is not optimal; i.e., the beam is not at its waist at the end of the matching section. Nevertheless, this matching section eases the requirement on the downstream beam transport. The simulation using the density profile shown by the red line in the top row in Fig. 1(b) gives similar results.

VI. CONCLUSIONS

We have investigated the generation of ultralow-emittance, high-brightness beams using a high-energy, high-current beam driver such as that available at FACET II to excite a wake across a density down ramp. The shock-front-induced down ramps were experimentally characterized, and the results show that the lower shelf density of the down ramp can be changed linearly from 10^{18} to 4×10^{18} cm^{-3}, the density ratio between the upper shelf and the lower shelf is 2–3, and the ramp length is ~10 c/ω_p. We then show using 3D PIC simulations that beams with a slice emittance as low as ~35 nm can be injected using such ramps. The peak current of the beam is ~10 kA, corresponding to a brightness of 10^{19} A/m^2/rad^2. The measurements show that the down ramp length varies within the range of 5–15 c/ω_p as the plasma source condition changes, which may cause the emittance to change in the range of ~0.03–0.1 μm according to the simulation. For a given condition (e.g., a fixed backing pressure and/or a particular height above the nozzle exit), the ramp length and the density drop fluctuate on the level of ~20%, which may lead to observable fluctuations in the emittance of the injected beam. The current profile of the injected beam is primarily determined by the density drop across the down ramp and is insensitive to the ramp length. Therefore, we expect only small fluctuations in the charge of the injected beam, since the density drop of the down ramp is quite reproducible. We also show using simulations that the current profile can be tuned by changing the shape of the down ramp. The effect of the noncylindrical drive beam has also been investigated. The slice emittance of the beam injected in the noncylindrical driver case is ~1 μm. A full-scale 2D simulation shows that using this scheme a low-emittance beam can be injected and accelerated to ~0.2 GeV in 4 mm and be matched out from the plasma with its emittance preserved.

ACKNOWLEDGMENTS

The simulations were performed on the Cori cluster at the National Energy Research Scientific Computing Center. This work was supported by the Department of Energy under Grant No. DE-SC0010064 and the National Science Foundation under Grant No. 1734315.

[1] M. Litos *et al.*, High-efficiency acceleration of an electron beam in a plasma wakefield accelerator, Nature (London) **515**, 92 (2014).

[2] O. Lundh, J. Lim, C. Rechatin, L. Ammoura, A. Ben-Ismaïl, X. Davoine, G. Gallot, J.-P. Goddet, E. Lefebvre, V. Malka, and J. Faure, Few femtosecond, few kiloampere electron bunch produced by a laser–plasma accelerator, Nat. Phys. **7**, 219 (2011).

[3] A. J. Gonsalves *et al.*, Petawatt Laser Guiding and Electron Beam Acceleration to 8 GeV in a Laser-Heated Capillary Discharge Waveguide, Phys. Rev. Lett. **122**, 084801 (2019).

[4] S. Corde *et al.*, Multi-gigaelectronvolt acceleration of positrons in a self-loaded plasma wakefield, Nature (London) **524**, 442 (2015).

[5] C. B. Schroeder, E. Esarey, C. G. R. Geddes, C. Benedetti, and W. P. Leemans, Physics considerations for laser-plasma linear colliders, Phys. Rev. Accel. Beams **13**, 101301 (2010).

[6] K. Nakajima, Towards a table-top free-electron laser, Nat. Phys. **4**, 92 (2008).

[7] H.-P. Schlenvoigt, K. Haupt, A. Debus, F. Budde, O. Jäckel, S. Pfotenhauer, H. Schwoerer, E. Rohwer, J. G. Gallacher, E. Brunetti, R. P. Shanks, S. M. Wiggins, and D. A. Jaroszynski, A compact synchrotron radiation source driven by a laser-plasma wakefield accelerator, Nat. Phys. **4**, 130 (2008).

[8] S. Cipiccia *et al.*, Gamma-rays from harmonically resonant betatron oscillations in a plasma wake, Nat. Phys. **7**, 867 (2011).

[9] S. Corde, K. T. Phuoc, G. Lambert, R. Fitour, V. Malka, A. Rousse, A. Beck, and E. Lefebvre, Femtosecond x rays from laser-plasma accelerators, Rev. Mod. Phys. **85**, 1 (2013).

[10] A. Döpp, B. Mahieu, A. Lifschitz, C. Thaury, A. Doche, E. Guillaume, G. Grittani, O. Lundh, M. Hansson, J. Gautier, M. Kozlova, J. P. Goddet, P. Rousseau, A. Tafzi, V. Malka, A. Rousse, S. Corde, and K. T. Phuoc, Stable femtosecond X-rays with tunable polarization from a laser-driven accelerator, Light Sci. Appl. **6**, e17086 (2017).

[11] J. Wenz, S. Schleede, K. Khrennikov, M. Bech, P. Thibault, M. Heigoldt, F. Pfeiffer, and S. Karsch, Quantitative X-ray phase-contrast microtomography from a compact laser-driven betatron source, Nat. Commun. **6**, 7568 (2015).

[12] S. Kneip, C. McGuffey, F. Dollar, M. S. Bloom, V. Chvykov, G. Kalintchenko, K. Krushelnick, A. Maksimchuk, S. P. D. Mangles, T. Matsuoka, Z. Najmudin, C. A. J. Palmer,

J. Schreiber, W. Schumaker, A. G. R. Thomas, and V. Yanovsky, X-ray phase contrast imaging of biological specimens with femtosecond pulses of betatron radiation from a compact laser plasma wakefield accelerator, Appl. Phys. Lett. **99**, 093701 (2011).

[13] J. M. Cole *et al.*, High-resolution μCT of a mouse embryo using a compact laser-driven X-ray betatron source, Proc. Natl. Acad. Sci. U.S.A. **115**, 6335 (2018).

[14] Z. Huang, Y. Ding, and C. B. Schroeder, Compact X-ray Free-Electron Laser from a Laser-Plasma Accelerator Using a Transverse-Gradient Undulator, Phys. Rev. Lett. **109**, 204801 (2012).

[15] T. Ishikawa *et al.*, A compact X-ray free-electron laser emitting in the sub-ångström region, Nat. Photonics **6**, 540 (2012).

[16] B. Hidding, G. Pretzler, J. B. Rosenzweig, T. Königstein, D. Schiller, and D. L. Bruhwiler, Ultracold Electron Bunch Generation via Plasma Photocathode Emission and Acceleration in a Beam-Driven Plasma Blowout, Phys. Rev. Lett. **108**, 035001 (2012).

[17] X. L. Xu, J. F. Hua, F. Li, C. J. Zhang, L. X. Yan, Y. C. Du, W. H. Huang, H. B. Chen, C. X. Tang, W. Lu, P. Yu, W. An, C. Joshi, and W. B. Mori, Phase-Space Dynamics of Ionization Injection in Plasma-Based Accelerators, Phys. Rev. Lett. **112**, 035003 (2014).

[18] Y. Wan, C. J. Zhang, F. Li, Y. P. Wu, J. F. Hua, C.-H. Pai, W. Lu, Y. Q. Gu, X. L. Xu, C. Joshi, and W. B. Mori, Colliding ionization injection in a plasma wakefield accelerator, Plasma Phys. Controlled Fusion **58**, 034015 (2016).

[19] F. Li, J. F. Hua, X. L. Xu, C. J. Zhang, L. X. Yan, Y. C. Du, W. H. Huang, H. B. Chen, C. X. Tang, W. Lu, C. Joshi, W. B. Mori, and Y. Q. Gu, Generating High-Brightness Electron Beams via Ionization Injection by Transverse Colliding Lasers in a Plasma-Wakefield Accelerator, Phys. Rev. Lett. **111**, 015003 (2013).

[20] A. Pak, K. A. Marsh, S. F. Martins, W. Lu, W. B. Mori, and C. Joshi, Injection and Trapping of Tunnel-Ionized Electrons into Laser-Produced Wakes, Phys. Rev. Lett. **104**, 025003 (2010).

[21] C. E. Clayton, J. E. Ralph, F. Albert, R. A. Fonseca, S. H. Glenzer, C. Joshi, W. Lu, K. A. Marsh, S. F. Martins, W. B. Mori, A. Pak, F. S. Tsung, B. B. Pollock, J. S. Ross, L. O. Silva, and D. H. Froula, Self-Guided Laser Wakefield Acceleration beyond 1 GeV using Ionization-Induced Injection, Phys. Rev. Lett. **105**, 105003 (2010).

[22] C. Thaury, E. Guillaume, A. Lifschitz, K. Ta Phuoc, M. Hansson, G. Grittani, J. Gautier, J.-P. Goddet, A. Tafzi, O. Lundh, and V. Malka, Shock assisted ionization injection in laser-plasma accelerators, Sci. Rep. **5**, 16310 (2015).

[23] X. L. Xu, F. Li, W. An, T. N. Dalichaouch, P. Yu, W. Lu, C. Joshi, and W. B. Mori, High quality electron bunch generation using a longitudinal density-tailored plasma-based accelerator in the three-dimensional blowout regime, Phys. Rev. Accel. Beams **20**, 111303 (2017).

[24] K. Schmid, A. Buck, C. M. S. Sears, J. M. Mikhailova, R. Tautz, D. Herrmann, M. Geissler, F. Krausz, and L. Veisz, Density-transition based electron injector for laser driven wakefield accelerators, Phys. Rev. Accel. Beams **13**, 091301 (2010).

[25] A. Buck, J. Wenz, J. Xu, K. Khrennikov, K. Schmid, M. Heigoldt, J. M. Mikhailova, M. Geissler, B. Shen, F. Krausz, S. Karsch, and L. Veisz, Shock-Front Injector for High-Quality Laser-Plasma Acceleration, Phys. Rev. Lett. **110**, 185006 (2013).

[26] S. K. Barber, J. van Tilborg, C. B. Schroeder, R. Lehe, H.-E. Tsai, K. K. Swanson, S. Steinke, K. Nakamura, C. G. R. Geddes, C. Benedetti, E. Esarey, and W. P. Leemans, Measured Emittance Dependence on the Injection Method in Laser Plasma Accelerators, Phys. Rev. Lett. **119**, 104801 (2017).

[27] K. K. Swanson, H.-E. Tsai, S. K. Barber, R. Lehe, H.-S. Mao, S. Steinke, J. van Tilborg, K. Nakamura, C. G. R. Geddes, C. B. Schroeder, E. Esarey, and W. P. Leemans, Control of tunable, monoenergetic laser-plasma-accelerated electron beams using a shock-induced density downramp injector, Phys. Rev. Accel. Beams **20**, 051301 (2017).

[28] H.-E. Tsai, K. K. Swanson, S. K. Barber, R. Lehe, H.-S. Mao, D. E. Mittelberger, S. Steinke, K. Nakamura, J. van Tilborg, C. Schroeder, E. Esarey, C. G. R. Geddes, and W. Leemans, Control of quasi-monoenergetic electron beams from laser-plasma accelerators with adjustable shock density profile, Phys. Plasmas **25**, 043107 (2018).

[29] S. Corde, C. Thaury, A. Lifschitz, G. Lambert, K. Ta Phuoc, X. Davoine, R. Lehe, D. Douillet, A. Rousse, and V. Malka, Observation of longitudinal and transverse self-injections in laser-plasma accelerators, Nat. Commun. **4**, 1501 (2013).

[30] J. Grebenyuk, A. M. de la Ossa, T. Mehrling, and J. Osterhoff, Beam-driven plasma-based acceleration of electrons with density down-ramp injection at FLASHForward, Nucl. Instrum. Methods Phys. Res., Sect. A **740**, 246 (2014).

[31] A. Deng *et al.*, Generation and acceleration of electron bunches from a plasma photocathode, Nat. Phys. https://doi.org/10.1038/s41567-019-0610-9 (2019).

[32] C. Joshi, E. Adli, W. An, C. E. Clayton, S. Corde, S. Gessner, M. J. Hogan, M. Litos, W. Lu, K. A. Marsh, W. B. Mori, N. Vafaei-Najafabadi, B. O'shea, X. Xu, G. White, and V. Yakimenko, Plasma wakefield acceleration experiments at FACET II, Plasma Phys. Controlled Fusion **60**, 034001 (2018).

[33] M.-W. Lin, Y.-M. Chen, C.-H. Pai, C.-C. Kuo, K.-H. Lee, J. Wang, S.-Y. Chen, and J.-Y. Lin, Programmable fabrication of spatial structures in a gas jet by laser machining with a spatial light modulator, Phys. Plasmas **13**, 110701 (2006).

[34] G. Wittig, O. S. Karger, A. Knetsch, Y. Xi, A. Deng, J. B. Rosenzweig, D. L. Bruhwiler, J. Smith, Z.-M. Sheng, D. A. Jaroszynski, G. G. Manahan, and B. Hidding, Electron beam manipulation, injection and acceleration in plasma wakefield accelerators by optically generated plasma density spikes, Nucl. Instrum. Methods Phys. Res., Sect. A **829**, 83 (2016).

[35] R. A. Fonseca, L. O. Silva, F. S. Tsung, V. K. Decyk, W. Lu, C. Ren, W. B. Mori, S. Deng, S. Lee, T. Katsouleas, and J. C. Adam, in *Computational Science—ICCS 2002*, edited by P. M. A. Sloot, A. G. Hoekstra, C. J. K. Tan, and J. J. Dongarra (Springer, Berlin, 2002), pp. 342–351.

[36] H. Ekerfelt, M. Hansson, I. G. González, X. Davoine, and O. Lundh, A tunable electron beam source using trapping of electrons in a density down-ramp in laser wakefield acceleration, Sci. Rep. **7**, 12229 (2017).

[37] A. M. de la Ossa, Z. Hu, M. J. V. Streeter, T. J. Mehrling, O. Kononenko, B. Sheeran, and J. Osterhoff, Optimizing density down-ramp injection for beam-driven plasma wakefield accelerators, Phys. Rev. Accel. Beams **20**, 091301 (2017).

[38] S. Wilks, T. Katsouleas, J. M. Dawson, P. Chen, and J. J. Su, Beam loading in plasma waves, IEEE Trans. Plasma Sci. **15**, 210 (1987).

[39] W. Lu, M. Tzoufras, C. Joshi, F. S. Tsung, W. B. Mori, J. Vieira, R. A. Fonseca, and L. O. Silva, Generating multi-GeV electron bunches using single stage laser wakefield acceleration in a 3D nonlinear regime, Phys. Rev. Accel. Beams **10**, 061301 (2007).

[40] M. Tzoufras, W. Lu, F. S. Tsung, C. Huang, W. B. Mori, T. Katsouleas, J. Vieira, R. A. Fonseca, and L. O. Silva, Beam Loading in the Nonlinear Regime of Plasma-Based Acceleration, Phys. Rev. Lett. **101**, 145002 (2008).

[41] T. Katsouleas, Physical mechanisms in the plasma wakefield accelerator, Phys. Rev. A **33**, 2056 (1986).

[42] B. Jiang, C. Jing, P. Schoessow, J. Power, and W. Gai, Formation of a novel shaped bunch to enhance transformer ratio in collinear wakefield accelerators, Phys. Rev. Accel. Beams **15**, 011301 (2012).

[43] G. Loisch *et al.*, Observation of High Transformer Ratio Plasma Wakefield Acceleration, Phys. Rev. Lett. **121**, 064801 (2018).

[44] Q. Gao, G. Ha, C. Jing, S. P. Antipov, J. G. Power, M. Conde, W. Gai, H. Chen, J. Shi, E. E. Wisniewski, D. S. Doran, W. Liu, C. E. Whiteford, A. Zholents, P. Piot, and S. S. Baturin, Observation of High Transformer Ratio of Shaped Bunch Generated by an Emittance-Exchange Beam Line, Phys. Rev. Lett. **120**, 114801 (2018).

[45] X. L. Xu, J. F. Hua, Y. P. Wu, C. J. Zhang, F. Li, Y. Wan, C.-H. Pai, W. Lu, W. An, P. Yu, M. J. Hogan, C. Joshi, and W. B. Mori, Physics of Phase Space Matching for Staging Plasma and Traditional Accelerator Components using Longitudinally Tailored Plasma Profiles, Phys. Rev. Lett. **116**, 124801 (2016).

[46] R. D'Arcy *et al.*, Tunable Plasma-Based Energy Dechirper, Phys. Rev. Lett. **122**, 034801 (2019).

[47] V. Shpakov *et al.*, Longitudinal Phase-Space Manipulation with Beam-Driven Plasma Wakefields, Phys. Rev. Lett. **122**, 114801 (2019).

[48] Y. P. Wu, J. F. Hua, Z. Zhou, J. Zhang, S. Liu, B. Peng, Y. Fang, Z. Nie, X. N. Ning, C.-H. Pai, Y. C. Du, W. Lu, C. J. Zhang, W. B. Mori, and C. Joshi, Phase Space Dynamics of a Plasma Wakefield Dechirper for Energy Spread Reduction, Phys. Rev. Lett. **122**, 204804 (2019).